Iranian Journal of Hydrogen & Fuel Cell 9(2022) 107-116

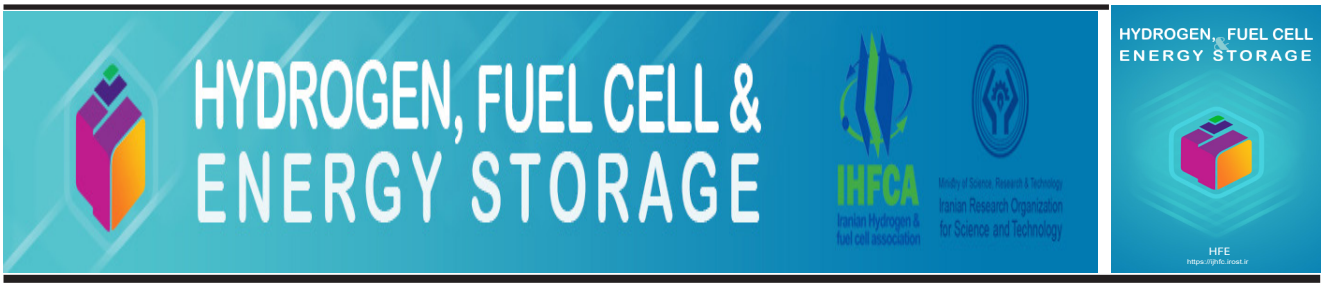

Numerical-experimental study on the Failure Behavior of Graphite-Based Composite Bipolar Plate for PEM fuel cells

L. Emami[1], M. M. Barzegari[2,*], M. R. Zamani[1,*], J. Eskandarijam[1]

[1] Faculty of Manufactured Materials and Technologies, Malek Ashtar University of Technology, Iran
[2] Northern Research Center for Science and Technology, Malek Ashtar University of Technology, Iran

Article Information

Article History:

Received:
31 Jul 2022
Received in revised form:
26 Sep 2022
Accepted:
07 Oct 2022

Keywords

PEM Fuel Cell
Composite Bipolar Plate
Three-Point bending
Finite Element Simulation

Abstract

In this study, the fracture method is used to numerically and experimentally investigate the bending load of graphite-based composite bipolar plates of polymer electrolyte membrane fuel cells. First, simple and perforated composite bipolar plates were tested and simulated to determine flexural stability under static load. Then, mechanical simulation using the finite element method and Abaqus software was used for the numerical analysis. Next, an experimental three-point bending test was performed on the manufactured samples to validate the simulation results. Finally, the results of the numerical and experimental analyzes of the flexural behavior of composite bipolar plates were compared. The results demonstrated that the numerical results acceptably agreed with the experimental data. In addition, the presence of a high percentage of graphite and high fragility weakened the body due to the molecular bond of graphite, which caused the graphite to slip.

1. Introduction

As an energy generator, a polymer electrolyte membrane fuel cell (PEMFC) converts the chemical energy of the fuel directly into electrical energy. The bipolar plates (BPPs) are a critical component of PEMFC; they are responsible for the distribution of fuel and oxidants, facilitating water management inside the cell, and transmitting electric current. The bipo-

*Corresponding Author: : Barzegari@mut.ac.ir, a_mrzamani@mut.ac.ir

doi:10.22104/IJHFC.2022.5780.1241

lar plates collect the anode and cathode output current into the fuel cell. They are also a device for distributing fuel flow to the anode side and oxygen or air to the cathode side [1].

BPPs account for 60-80 % of the total weight of a polymer electrolyte membrane (PEM) fuel cell stack and 20-30 % of its manufacturing cost. Therefore, PEMFC stack cost and performance could be considerably enhanced by determining the mechanical properties of bipolar plates [2].

Metallic BPPs are preferred for commercial mass applications due to their excellent mechanical strength, as well as high electrical and thermal conductivity. However, their insufficient chemical stability in the PEMFC environment is a major limitation. Corrosion products that form on the surface of the BPP, specifically metal ions, poison the fuel cell membrane and anode, resulting in the degradation of stack efficiency [3, 4]. Barzegari et al. [5] investigated the morphology and electrical and electrochemical properties of gold plating on metal bipolar plates of polymer fuel cells. The properties and morphology of gold coating on copper and stainless-steel substrates were studied using electroplating and spattering methods. Their results showed that the use of the electrical plating method causes many holes increasing the surface porosity of the specimens. Belali et al. [6] experimentally and numerically examined stainless steel bipolar plates with a pin pattern using a convex hydroforming process. They changed various parameters such as applied pressure level, pin geometry, and depth to width ratio and compared results such as formed profiles, filling percentage, thickness distribution, and thinning percentage of formed profiles.

In general, the results showed that polymer-carbon composites have a lower density than metallic plates but need to be thicker because of their lower mechanical strength, which results in polymer-carbon BPPs stacks having a lower power density [7].

In recent years, extensive studies have been conducted to investigate the behavior and enhance the characteristics of graphite-based composite bipolar plates. Chen et al. [8] conducted a study to prepare bipolar plates based on graphite/resin for a fuel cell. They found that composite plates that used epoxy resin as a receiver had better electrical conductivity, flexural strength, and overall properties than those using single-phenolic resin. Okhawilai et al. [9] studied the effect of graphite and graphene on a bipolar plate filled with polybasoboxazine in the fuel cell. They tried to find ways to improve the characteristics of this type of page by expressing the disadvantages and advantages. They concluded that using pure graphite dipole plates was restrictive due to poor mechanical properties and high production costs. Kang et al. [10] achieved an acceptable bending strength by designing and manufacturing a bipolar plate made of composite material with carbon fibers produced by pressure casting. Khaerudini et al. [11] investigated the effect of adding graphite on rolled shells waste to produce a material for making bipolar plates. They studied the use of rolled shells (a by-product of iron and steel produced during the hot rolling of steel) to make bipolar plates in the proton exchange membrane fuel cell. Hardness evaluation showed that much purer specimens than graphites should be added to achieve acceptable mechanical strength.

Radzuan et al. [12] studied the effect of fiber orientation on shredded polypropylene/carbon fiber composites in the presence of carbon or graphene nanotubes as a secondary filler in a bipolar plate. They performed studies using X-ray analysis methods to determine the effect of filler conductivity on electrical conductivity and the effect of filler orientation on mechanical properties. The results showed that the higher aspect ratio of carbon nanotubes was able to bring the filler up to 90% closer to the separation orientation, improving and enhancing the electrical conductivity at the surface and in the direction of thickness. Liang et al. [13] investigated the structural optimization of graphite for

a high-performance fluorinated ethylene/propylene composite bipolar plate. They presented a new method for structural optimization using graphite particles with sizes of 35 to 500 mm to make conductive fluorinated ethylene propylene composites for high-temperature bipolar plates. Their proposed method for producing graphite composite bipolar plates could also be used in the preparation of high-temperature bipolar plates for fuel cells and cooling components in electronic devices and automobile-related devices. According to studies, the mechanical properties of the bipolar plates have a significant effect on the failure of these plates. In this study, bipolar plates with and without grooves under loading and bending have been studied numerically and experimentally. Moreover, the results of the numerical and experimental analyzes of the flexural behavior of composite bipolar plates were compared.

2. Method of analysis

The beam was considered in accordance with the AStM D790 standard. Rectangular geometry with dimensions of 3 × 10 × 100 mm was considered. The diameter of the bending pins used in this test was 20 mm and the distance between the supports was 29 mm. The physical and mechanical properties of the composite material are shown in Table1 and Table 2.

Table 1. Name and percentage of materials BMC 940-8649 [14].

Material	Percent
Graphite	20-25
Styrene	5-10
Carbon	1-5
Methylene Diphenyl Diisocyate	1-5
Divinylbenzene	0.1-1
Benzene	0.1-1

Table 2. Mechanical properties of BMC 940-8649 [14].

Mechanical properties	Value	Unit
Young's modulus	11	GPa
Poisson's ratio	0.32	--
Ultimate tensile strength	30	MPa
Flexural strength	10.35	GPa
Flexural strength	40	MPa
Compressive strength	75	MPa
Density	1.84	g/cm^3

2.1. Finite-element modeling

For static load analysis, static and quasi-static analysis have been used in finite-element modeling in Abaqus software. In this analysis, the maximum bending force of the beam is investigated using a three-point bending test carried out with a static load. In order to simulate the three-point bending test, the parts were created and placed in the correct geometric position in relation to the system of unit coordinates. The element used is a C3D8R cube, representing an eight-node three-dimensional cube element (Fig. 1).

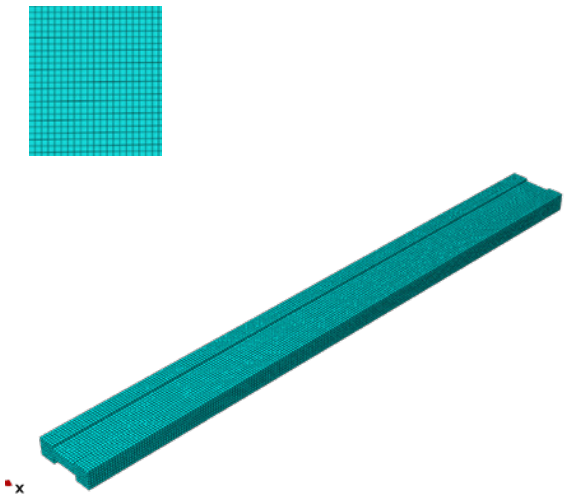

Fig. 1. Numerical Model meshing.

2.2. Experimental tests

In this section, the tested specimens were prepared according to the dimensions specified in the standard and related operations, i.e., the production of grooves using a CNC milling machine. Fig. 2 illustrates the fabricated component.

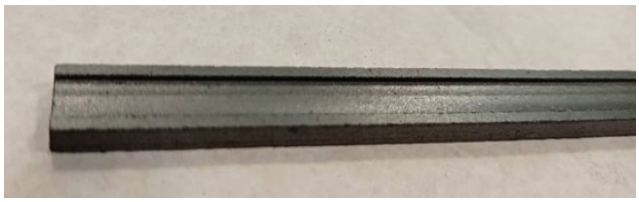

Fig.2. Grooved beam.

Specimens with a rectangular cross-section were used as beams. First, the specimens were placed on two supports at a specified distance. Then, using a mandrel from above and in the middle of these two supports, a force was applied to the center of the beam at a speed of 0.5 mm/min. The amount of flexural strength and modulus can be determined by measuring the deflection of the beam and the force applied to it.

After completing the numerical simulation using finite element software, the numerical method was compared and validated with the experimental test method via a bending machine with a capacity of 2000 kg (Fig. 3).

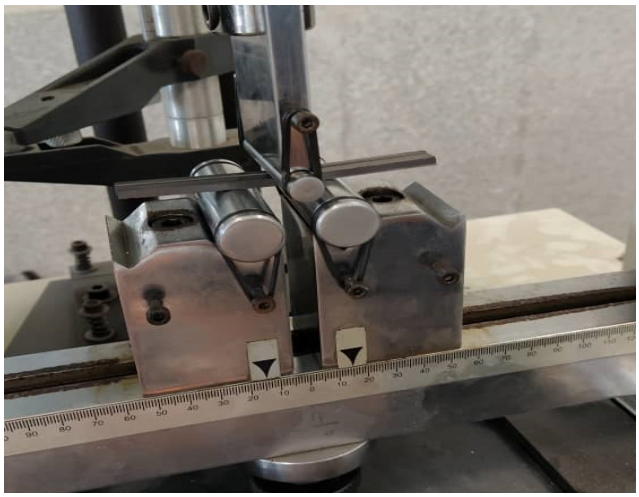

Fig. 3. Experimental setup for the three-point bending test.

According to the AStM D790 standard, the following equations can be used to determine the flexural modulus and strength.

$$\sigma_f = \frac{3Pl}{2bd^2} \quad (1)$$

$$E_B = \frac{L^3 m}{4bd^3} \quad (2)$$

Where σ_f is the flexural strength, E is the flexural modulus, P is the maximum force obtained from the force-displacement diagram, L is the distance between two supports, b is the width of the test specimen, d is the thickness of the specimen, and m is the slope of the tangent line to the linear part of the force-displacement diagram. Fig. 4 shows the dimensional characteristics of the tested specimens.

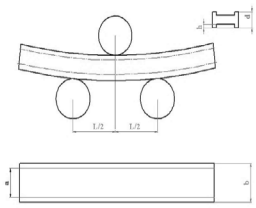

Fig. 4. Test of specimens.

Due to the specificity of the type of material and the presence of grooves, the Marciniak-Kuczynski (M-K) criterion has been used to predict the damage initiation. This approach can be used with Mises and Johnson-Cook plasticity models, including kinematic hardening. In M-K analysis, virtual thickness imperfections are introduced as grooves to simulate pre-existing defects in otherwise uniform sheet material. The deformation field is computed inside each groove as a result of the applied loading outside the groove. Necking is considered to occur when the ratio of the

deformation in the groove relative to the nominal deformation (outside the groove) is greater than a critical value.

Abaqus/Explicit analysis allows the specification of an anisotropic distribution of thickness imperfections as a function of angle with respect to the local material orientation, $f_0(\theta)$. Abaqus/Explicit first solves for the stress-strain field in the nominal area, ignoring the presence of imperfections; then, it considers the effect of each groove alone. Then, the deformation field inside each groove is computed by enforcing the strain compatibility condition:

$$\varepsilon_{tt}^{b} = \varepsilon_{tt}^{a} \tag{3}$$

and the force equilibrium equations:

$$F_{nn}^{b} = F_{nn}^{a} \tag{4}$$

$$F_{nt}^{b} = F_{nt}^{a} \tag{5}$$

The subscripts n and t refer to the directions normal and tangential to the groove. In the above equilibrium equations F_{nn} and F_{nt} are forces per unit width in the *t*-direction.

The onset of necking instability is assumed to occur when the ratio of the rate of deformation inside a groove relative to the rate of deformation if no groove were present is greater than a critical value. However, finding a solution that satisfies equilibrium and compatibility conditions may not be possible once localization initiates at a particular groove; consequently, failure to find a converged solution is also an indicator of the onset of localized necking. To evaluate the damage initiation criterion, Abaqus/Explicit uses the following measures of deformation severity:

$$f_{eq} = \frac{\Delta\varepsilon_{b}^{-pl}}{\Delta\varepsilon_{a}^{-pl}} \tag{6}$$

$$f_{nt} = \frac{\Delta\varepsilon_{nt}^{-b}}{\Delta\varepsilon_{nt}^{-a}} \tag{7}$$

These deformation severity factors are evaluated in each of the specified groove directions and compared with the critical values. It should be noted that the evaluation is performed only if the incremental deformation is primarily plastic; the M-K criterion will not predict damage initiation if the deformation increment is elastic. The most unfavorable groove direction is used for the evaluation of the damage initiation criterion, which is given as:

$$W_{MK} = \max\left(\frac{f_{eq}}{f_{eq}^{crit}}, \frac{f_{nn}}{f_{nn}^{crit}}, \frac{f_{nt}}{f_{nt}^{crit}}\right) \tag{8}$$

where f_{eq}^{crit} , f_{nn}^{crit} , and f_{nt}^{crit} are the critical values of the deformation severity indices. Damage initiation occurs when $W_{MK}=1$ or when a converged solution to the equilibrium and compatibility equations cannot be found. By default, Abaqus/Explicit assumes $f_{eq}^{crit}=f_{nn}^{crit}=f_{nt}^{crit}=10$; different values can be specified. If one of these parameters is set equal to zero, its corresponding deformation severity factor is not included in the evaluation of the damage initiation criterion [15].

3. Results and discussion

The groove creates a geometric discontinuity in the beam and reduces the strength of the beam. In this research, the effect of creating grooves on the surface of the beam with different depths and dimensions has been investigated. Due to the material's specificity and grooves' presence, the M-K Damage failure criterion has been used.

This criterion is calculated using equations of deformation compatibility and the equations of force equi-

librium. The determining factors of this criterion are:

- Groove size (which is calculated from the ratio of groove thickness to total thickness)
- Groove angle (groove angle is 90 degrees here)
- Failure energy
- The exact amount of plastic

3.1. Comparison of the numerical and experimental analysis of a simple beam

In order to obtain the best numerical resolution results, this analysis was carried out with a number of different elements. The results reached convergence when the number of considered elements increased to 15,000. Fig. 5 shows the mesh convergence diagram.

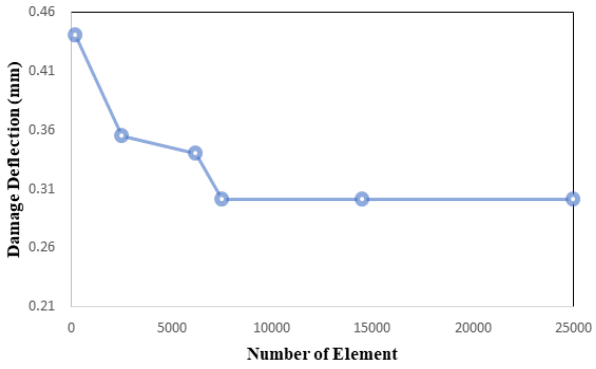

Fig. 5. Mesh convergence.

This section compared the experimental analysis and numerical results of flexural loading. Fig. 6 compares the force-displacement diagram of a simple beam's numerical and experimental results with a relatively good difference percentage. A comparison of a simple bean's numerical and experimental analysis results indicates that the maximum tolerable force in the numerical model is 126 N and 120 N in the experimental specimens. With a difference of 9%, it shows almost good convergence.

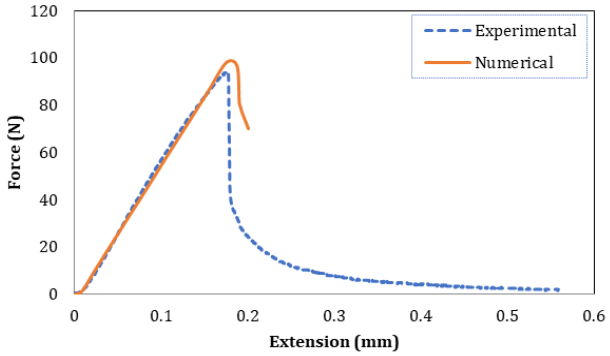

Fig. 6. Comparison of numerical and experimental results of a simple beam.

The comparison of the flexural properties of a simple beam is shown in Table 3.

Table 3. Comparison of flexural properties of a simple beam.

Geometry	Deflection (mm)	Bending modulus (GPa)	Ultimate strength (MPa)	Error (%)
Simple beam	Numerical	0.22	14.452	58.567
100×10×3 mm	Experimental	0.29	14.600	56.600

9

Fig. 7 shows the contours of stress and strain resulting from the simulation of the three-point bending test for a perforated beam with a hole width of 2 and different lengths.

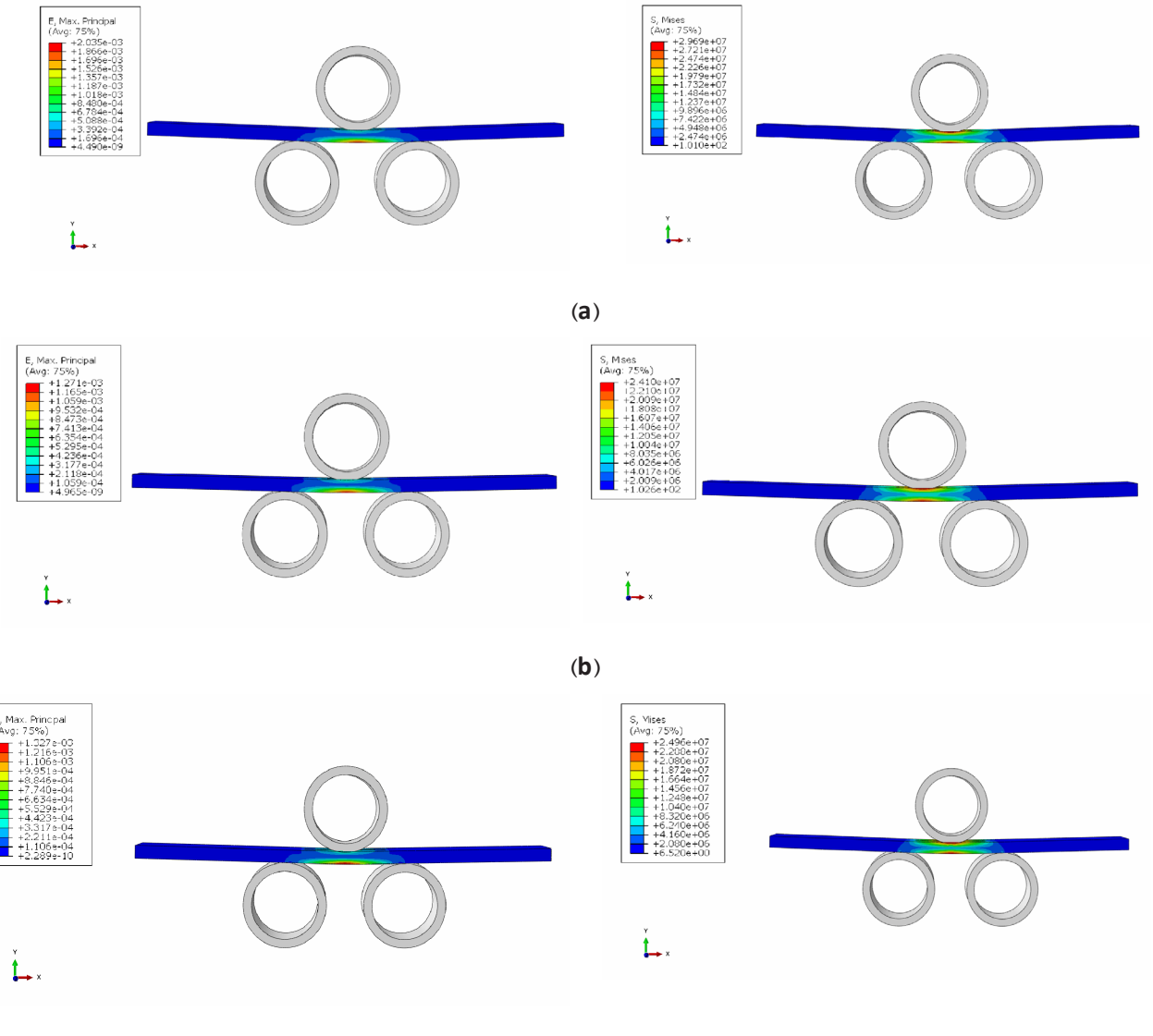

Fig. 7. Stress and strain contours of the perforated beam with a hole width of 2 and (a) 4, (b) 12, and (c) 20 mm.

3.2. Comparison of the numerical and experimental analysis of grooved beams

Figs. 8, 9, and 10 compare the numerical and experimental analysis of the beam with the groove at the bottom at a depth of 0.45 mm, at the top at a depth of 0.9, and in the two levels at a depth of 0.9 and 0.45, respectively. As can be seen, increasing the fracture force is directly related to increasing the flexural modulus and flexural strength, but the beam deformation decreases.

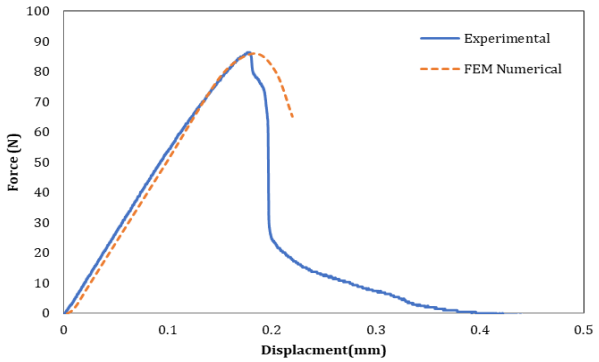

Fig. 8. Beam with a groove with a width of 4.7 and a depth of 0.45 mm at the bottom of the piece.

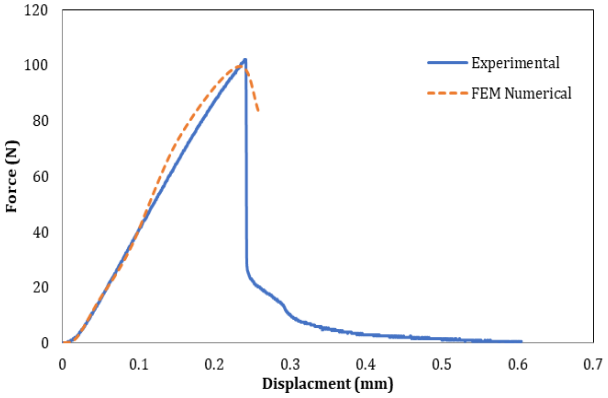

Fig. 9. Beam with a groove 4.7 in width and 0.9 mm deep in the top of the piece.

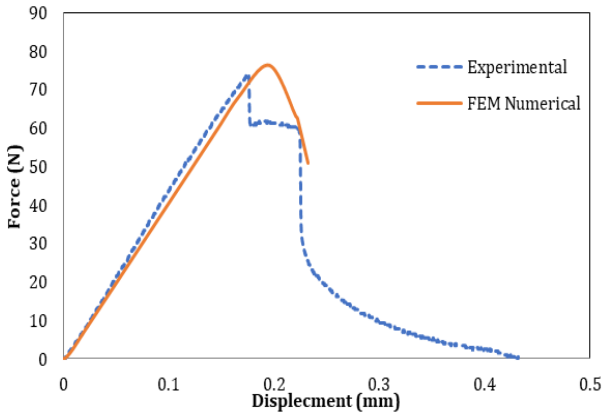

Fig. 10. Beam with a groove with a width of 4.7 and depth of 0.45 mm below the piece and a groove with a width of 4.7 and depth 0.9 mm above the piece.

Comparison of Figs. 8-10 shows a significant agreement in the numerical and experimental models and indicates the high accuracy of the numerical simulation.

The comparison of the flexural properties of the grooved beam is illustrated in Table 4.

Table 4. Comparison of flexural properties of the grooved beam.

Geometry	Deflection (mm)	Bending modulus (GPa)	Ultimate strength (MPa)	Error (%)	
Beam A	Numerical	0.183	12.08	42.208	8.09
	Experimental	0.180	11.968	41.541	
Beam B	Numerical	0.231	9.281	48.061	8
	Experimental	0.236	9.552	49.347	
Beam C	Numerical	0.202	7.880	32.324	6
	Experimental	0.210	7.428	35.814	

Beam A: Beam with a groove with a width of 4.7 and a depth of 0.45 mm at the bottom of the piece.

Beam B: Beam with groove 4.7 in width and 0.9 mm deep in the top of the piece.

Beam C: Beam with a groove with a width of 4.7 and depth of 0.45 mm below the piece and a groove with a width of 4.7 and depth of 0.9 mm above the piece.

Figs. 11 and 12 show the different positions of the groove on the beam with a width of 4.7 and 5.5, respectively. The three-point bending test of grooved beams in the upper grooves of the beam is subjected to compressive force, and the lower grooves are subjected to tensile force. Regardless of the groove depth, numerical and experimental results indicate that the tensile strength of the beams will be greatly reduced.

The reasons for the similarity of numerical and experimental results can be divided into the following categories:

- The high number of elements in the numerical simulation significantly helps converge the results.
- Another significant cause is the material, which is very brittle and lacks plastic behavior.

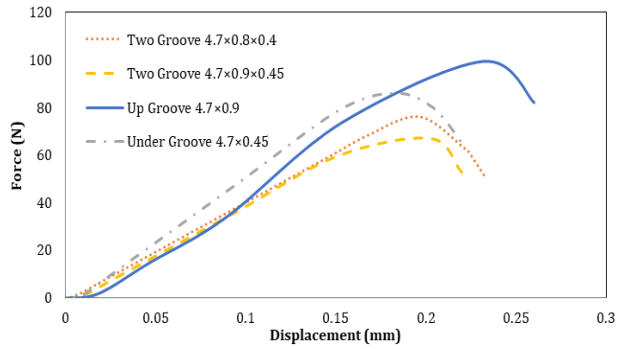

Fig. 11. Comparison of a beam with a width of 4.7 with four different groove modes.

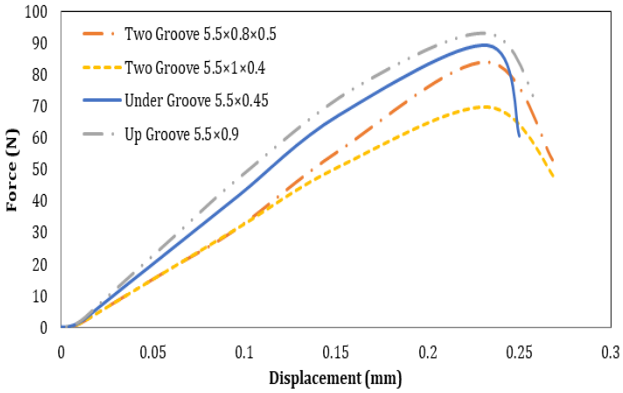

Fig. 12. Comparison of a beam with a width of 5.5 with four different groove modes.

4. Conclusion

In this research, composite bipolar plates have been investigated. For the flexural analysis, these plates were studied in composite beams with and without grooves using the flexural stability approach and determining the fracture strength. The obtained numerical and experimental results were compared in terms of flexural behavior. The investigated beams in the bending test were more vulnerable in the lower part because they were under tension, and as expected, the investigated beam was more resistant in the compression state than in the tensile state. Also, numerical and experimental analysis of these beams with this type of material had a higher deflection due to the greater percentage of graphics and were also more fragile, weakening the body. This problem only occurs due to the molecular bond of the graphic, which causes the graphic to slip. Also, the beam with the upper groove was observed to have more strength than the beam with the lower groove

References

[1] Barbir F, Yazici S. "Status and development of PEM fuel cell technology". International Journal of Energy Research. Vol. 32, No. 5, (2008), 369-78. DOI: 10.1002/er.1371.

[2] Thompson St, James BD, Huya-Kouadio JM, Houchins C, DeSantis DA, Ahluwalia R, et al. »Direct hydrogen fuel cell electric vehicle cost analysis: System and high-volume manufacturing description, validation, and outlook«. Journal of Power Sources. 2018;399:304-13. DOI:10.1016 /j.jpowsour.2018.07.100

[3] Porstmann S, Wannemacher T, Drossel WG. »A comprehensive comparison of state-of-the-artmanufacturing methods for fuel cell bipolar plates including anticipated future industry trends«. Journal of Manufacturing Processes. 2020;60:366-83. DOI: 10.1016/j.jmapro.2020.10.041.

[4] Dundar F, Dur E, Mahabunphachai S, Koç M. »Corrosion resistance characteristics of stamped and hydroformed proton exchange membrane fuel cell metallic bipolar plates«. Journal of Power Sources. 2010;195:3546-52. DOI:10.1016 /j.jpowsour.2009.12.040.

[5] Barzegari MM, Mohammadalitabar Khoshrodi A, Ghadimi M, Sedighi M. "Investigation of Morphology, Electrical and Electrochemical Properties of Gold Coating on Metallic Bipolar Plates of Fuel Cells" Advanced Materials and New Coatings, Vol. 8, No. 32, (2020), 2334-2335.

[6] Belali Owsia M, Jamal Hosseinipour S, Bakhshi Jooybari M, Gorji A. "Forming of metallic bipolar plate with pin-type pattern
by using hydroforming process in convex die" Modares Mechanical Engineering, Vol. 14, No. 10, (2015), 319-327.

[7] Saadat N, Dhakal HN, Tjong J, Jaffer S, Yang W, Sain M. Recent advances and future perspectives of carbon materials for fuel cell. Renewable and Sustainable Energy Reviews. 2021;138. DOI: 10.1016/j.rser.2020.110535.

[8] Chen, H., Xia, X. H., Yang, L., & Liu, H. B. "Preparation and characterization of graphite/resin composite bipolar plates for polymer electrolyte membrane fuel cells" Science and Engineering of Composite Materials, Vol. 23, No. 1, (2016), 21-28. DOI: 10.1515/secm-2013-0306.

[9] Okhawilai M, Pengdam A, Plengudomkit R, Rimdusit S. "Effects of Graphene and Graphite on Properties of Highly Filled Polybenzoxazine Bipolar Plate for Proton Exchange Membrane Fuel Cell: A Comparative Study" InCarbon-related Materials in Recognition of Nobel Lectures by Prof. Akira Suzuki in ICCE, (2017), 211-259. DOI: 10.1016/j.ijhydene.2020.08.006.

[10] Kang S.-J, Kim D. O., Lee J.-H, Lee P.-C, M.-H. Lee, Y.Lee, J. Y. Lee, H. R. Choi, J.-H. Lee, Y.-S. Oh, J.-D. Nam, Solvent-assisted graphite loading for highly conductive phenolic resin bipolar plates for proton exchange membrane fuel cells, Journal of Power Sources, 195(12), (2010), 3794-3801.

[11] Khaerudini DS, Prakoso GB, Insiyanda DR, Widodo H, Destyorini F, Indayaningsih N. "Effect of graphite addition into mill scale waste as a potential bipolar plates material of proton exchange membrane fuel cells" Journal of Physics: Conference Series, Vol. 985, No. 1, (2018), 120-126.

[12] Radzuan NA, Sulong AB, Somalu MR, Abdullah AT, Husaini T, Rosli RE, Majlan EH, Rosli MI. "Fibre orientation effect on polypropylene/milled carbon fiber composites in the presence of carbon nanotubes or graphene as a secondary filler: Application on PEM fuel cell bipolar plate" International journal of hydrogen energy. Vol. 44, No. 58, (2019), 30618-30626.

[13] Liang, P, Qiu, D, Peng, L, Yi, P, Lai, X, Ni, J. "Contact resistance prediction of proton exchange membrane fuel cell considering fabrication characteristics of metallic bipolar plates". Energy conversion and management, Vol. 169, 2, (2018), 334-344. DOI: 10.1016/j.enconman.2018.05.069

[14] www.Lyondollbadell.com

[15] Kacar, Ilyas, FAHRETTİN ÖZTÜRK, Serkan Toros, and Suleyman Kilic. "Prediction of strain limits via the marciniak-kuczynski model and a novel semi-empirical forming limit diagram model for dual-phase DP600 advanced high strength steel." Strojniski Vestnik/Journal of Mechanical Engineering. Vol.66, 10, (2020), 602-612. DOI:10.5545/sv-jme.2020.6755